Diamond Radio Receiver: Nitrogen-Vacancy Centers as Fluorescent Transducers of Microwave Signals

Linbo Shao,[1] Mian Zhang,[1] Matthew Markham,[2] Andrew M. Edmonds,[2] and Marko Lončar[1,*]

[1]*John A. Paulson School of Engineering and Applied Science, Harvard University, 29 Oxford Street, Cambridge, Massachusetts 02138, USA*

[2]*Element Six Global Innovation Centre, Fermi Avenue, Harwell Oxford, Didcot, Oxfordshire OX110QR, United Kingdom*

(Received 15 August 2016; revised manuscript received 12 October 2016; published 15 December 2016)

We demonstrate a robust frequency-modulated radio receiver using electron-spin-dependent photoluminescence of nitrogen-vacancy centers in diamond. The carrier frequency of the frequency-modulated signal is in the 2.8-GHz range, determined by the zero-field splitting in the nitrogen-vacancy electronic ground state. The radio can be tuned over 300 MHz by applying an external dc magnetic field. We show the transmission of high-fidelity audio signals over a bandwidth of 91 kHz using the diamond radio. We demonstrate operating temperature of the radio as high as 350 °C.

DOI: 10.1103/PhysRevApplied.6.064008

I. INTRODUCTION

From their first demonstration over a hundred years ago [1], radio waves have found numerous applications, with the most important being wireless communication [2,3]. In their simplest form, the radio transmitter imprints the signal to be transmitted onto the amplitude, frequency, or phase of the carrier signal, while the receiver demodulates the radio waves to retrieve the information. Many modern applications require small and robust receivers that could operate in high temperature (>100 °C), high pressure, and/or a chemically harsh environment. Recently, novel schemes capable of sensing radio-frequency electromagnetic waves have emerged, including those based on 2D materials [4,5], optomechanics [6–8], and nitrogen-vacancy (NV) centers in diamond [9–15]. Among these devices, diamond detectors are particularly interesting owing to the unique properties of diamonds. Diamond devices can operate in extremely challenging conditions, including high pressure up to 60 GPa (Ref. [16]), high temperature over 600 K (Ref. [17]), and a corrosive environment.

In this article, we demonstrate a diamond NV-based radio receiver that is capable of transducing frequency-modulated (FM) microwave radio signals to amplitude-modulated (AM) optical fluorescence signal. Our device takes advantage of the fact that the photoluminescence [18–20] of an NV center depends on its electron spin state, which is sensitive to microwave radiation. Transmission of high-fidelity audio is experimentally demonstrated and the bandwidth of the diamond radio receiver is measured to be 91 kHz. Furthermore, we show that the operating temperature of a diamond radio can be as high as 350 °C, much higher than that of a traditional integrated-circuit-based radio receiver (typical 85 °C for commercial products).

II. EXPERIMENTAL SETUP AND PRINCIPLE

The schematic of the NV radio receiver is depicted in Fig. 1(a). It is based on a bulk diamond sample (Element Six, HPTP diamond plate, with {100} faces) with a high density of NV centers (∼1.2 ppm with nitrogen concentration about 200–300 ppm, determined by absorption techniques in Ref. [21]). The diamond sample is then irradiated with 4.5 MeV electrons for 2 h, annealed at 800 °C for 16 h, and then at 1200 °C for 2 h. The diamond chip is continuously excited by a green (532 nm) laser; the excitation light spot is about 20 mW illuminating a 200-μm-diameter region at the surface of the diamond sample. An electromagnet is used to provide a dc magnetic field along axes of one NV class that defines the carrier frequency that the diamond receiver responds to. The microwave signal is delivered to the diamond chip by a microstrip waveguide contacting the surface of the diamond. The microstrip is microfabricated on a cover glass with a 20-μm width. The NV fluorescence, the output of the radio receiver, is collected by an objective (Olympus SLMPlan 50X/NA 0.35) and detected by a photodetector (New Focus 1801-FS) with filters (Semrock StopLine notch filter 532 nm, *E* grade, and Semrock EdgeBasic long-wavelength-pass filter, 632.8 nm). Compared with widely used pulsed laser experimental configuration [9–13], the continuous optical pumping [14,15] enables the continuous detection of the input microwave signal and enjoys the benefits of the high density of NV centers in bulk diamond. The high NV density gives a greater signal intensity and thus a better signal-to-noise ratio, even though the coherent time of dense NV centers could be shorter than the scattered NV centers in bulk diamond.

*loncar@seas.harvard.edu

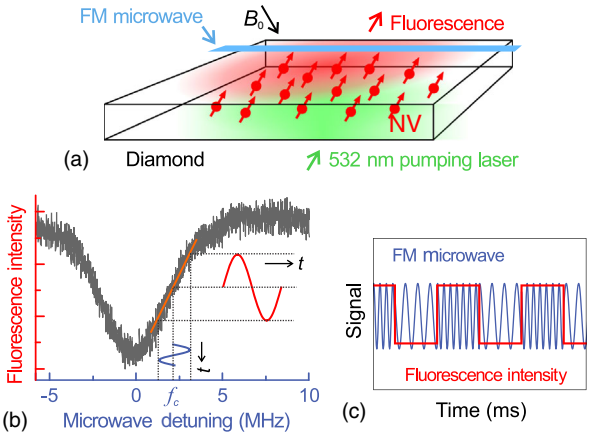

FIG. 1. (a) Experimental schematic of the nitrogen-vacancy (NV) radio receiver. The NV centers in diamond demodulate frequency-modulated (FM) microwave signals and map it onto the fluorescence. The NV centers are pumped by a green (532 nm) laser. The dc magnetic field B_0 is applied to tune the detecting carrier frequency of the microwave signal. (b) The principle of NV FM microwave demodulation. The black trace shows experimentally measured optically detected magnetic resonance (ODMR) near 2.87 GHz of NV centers. The fluorescence intensity depends on the detuning of the input microwave frequency from the ODMR resonance. The carrier frequency (f_c) is positioned on the slope, and changes in microwave frequency are mapped onto the changes in fluorescence intensity. (c) Illustration of the input FM microwave signal to be demodulated (blue) and resulting output amplitude-modulated fluorescence signal (red).

The FM discrimination in our device is achieved by the electron-spin-state-dependent fluorescence of NV centers. The negatively charged NV center is a lattice defect in diamond, which consists of a substitutional nitrogen atom and an adjacent vacancy. The ground state of the NV center is a spin triplet state, and the $m_s = \pm 1$ sublevels can be distinguished by their darker photoluminescence than the $m_s = 0$ sublevel due to the spin-selective intersystem crossing [17,20]. For clarity and simplicity, we only investigate the interaction between $m_s = -1$ and $m_s = 0$ sublevels. The sublevels in ground states are separated by

$$f_0 = D(T) - \gamma B_0, \tag{1}$$

where $D(T)$ is the crystal field splitting depending on the temperature T, which is about 2.87 GHz at room temperature, the gyromagnetic ratio $\gamma/2\pi$ of NV centers is 28 MHz/mT, B_0 is the dc magnetic field projected on the NV axis. As shown in Fig. 1(b), when the microwave frequency f_{MW} is swept over the resonance frequency f_0 of the NV ground sublevels, a dip in fluorescence intensity is observed. The principle of demodulating the FM microwave signal is as follows: when the carrier frequency is positioned on the slope of the dip, the frequency of the microwave signal is mapped onto the intensity modulation of the NV fluorescence. The optical (fluorescence) response of diamond chip exposed to an FM (square wave) microwave signal is depicted in Fig. 1(c).

III. EXPERIMENTAL RESULTS AND DISCUSSION

We demonstrate receiving FM radio signals carried by a 2.85-GHz carrier using the diamond NV centers. A known modulating signal (provided by a waveform generator, Agilent 33120A) representing the information is sent to a microwave function generator (HP ESG-3000A) to generate an FM microwave signal at the carrier frequency of 2.85 GHz with −3 dBm power. The microwave signal is then sent to the NV centers via a microstrip. The red fluorescence of NV centers is filtered, detected, and monitored by an oscilloscope with the modulating signal, as shown in Fig. 2. A dc magnetic field is applied by the electromagnet to shift the optically detected magnetic resonance (ODMR) dip to the position so that the carrier frequency is blue detuned from the NV microwave resonance. In this way, the received signal is in phase with the original modulating signal. From Figs. 2(a) and 2(b), we can conclude that the received signals are in good agreement with the modulating signals. As a demonstration of a real-life application, we transmit an audio signal and a demonstration of an audio transmission is provided as

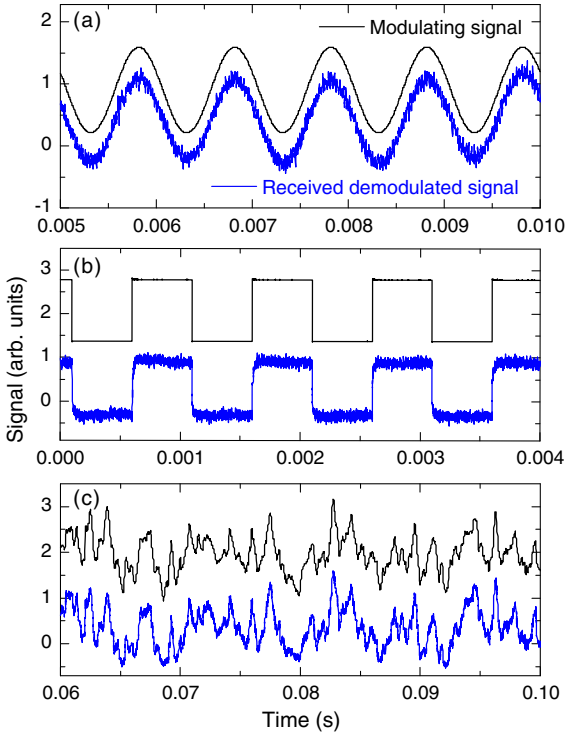

FIG. 2. The demodulated fluorescence intensities (shown in blue) compared to the original modulating signal (black). The curves are offset for clarity. In the case of (a) 1-kHz sine wave, (b) 1-kHz square wave, and (c) an audio signal. The carrier microwave is at 2.85 GHz.

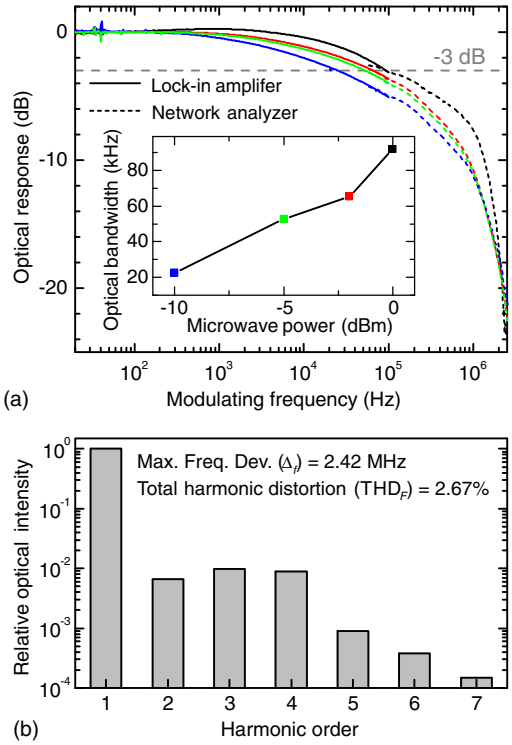

FIG. 3. (a) Optical response of an NV radio receiver on the frequency of modulating signals. The solid line is measured by the lock-in amplifier, and the dashed line is measured by the network analyzer. Lines of different color correspond to different carrier microwave powers indicated in the inset. Inset: dependency of −3 dB optical bandwidth on the powers of input microwave signals. (b) The harmonic distortion of the output fluorescence intensity in the case of a 1-kHz sine wave as a modulating signal with a maximum frequency deviation of $\Delta = 2.42$ MHz. The power of the microwave signal is −5 dBm.

Video S1 in the Supplemental Material [22]. As shown in Fig. 2(c), the received audio waveform is in good agreement with the original audio waveform.

We characterize the frequency responses of the NV radio for various microwave signal powers [Fig. 3(a)]. The modulating frequency of the carrier microwave signal is swept from 10 Hz to 3 MHz. Because of the limitation of detecting frequencies of the equipment, the 10-to-100-kHz response is measured by a lock-in amplifier (Stanford SR830), and are represented by solid lines in Fig. 3(a); while the 30-kHz-to-30-MHz frequencies are measured by a network analyzer (HP 8753E), and are represented by dashed lines in Fig. 3(a). The modulating signal is a sine wave with peak-to-peak amplitude $V_{PP} = 1$ V, and leads to the maximum deviation of 1 MHz from the frequency of the carrier microwave. As shown in Fig. 3(a), the −3-dB bandwidth of optical response is measured as 91.8 kHz with a microwave signal of 0 dBm (i.e., 1 mW), which is the maximum power that our microstrip can carry before being damaged. The carrier microwave frequency sits at the maximum slope of resonance dip, ensuring an optimum amplitude of the demodulated signal, as shown in Fig. 1(b). This bandwidth is adequate for high-fidelity audio transmission, as shown in Fig. 2(c). The bandwidth of the NV radio receiver is sensitive to the power of the input microwave signal. As plotted in Fig. 3(a), inset, the bandwidth is lowered from 91.8 to 22.5 kHz, when microwave signal power is attenuated from 0 to −10 dBm. The bandwidth also depends on other parameters including the pumping (green) laser power and detuning of the microwave carrier. An extensive discussion [23] of optical frequency response and bandwidth is presented by numerical simulations of NV center dynamics [20,24–28]. A simple rule of thumb is that greater pumping laser powers and microwave signal powers result in greater bandwidths, as shown in Figs. S4 and S5. The bandwidth might be extended by detuning of the carrier microwave from ODMR, as discussed in Fig. S3. However, the amplitude of the fluorescence signal suffers when the microwave frequency is detuned beyond one linewidth of the NV ground-state sublevels. The bandwidth of NV centers could be extended by changing the life time of states by strain [29].

We show the total harmonic distortion (THD) is 2.67% of the total signal at the microwave power of −5 dBm and a frequency deviation of 2.42 MHz, which is the half of the linewidth (as FWHM) of the NV microwave resonance in the ground state. In this case, the modulating signal is a 1-kHz sine wave, and the optical intensity (as the output of the photodetector) of the higher-order harmonic frequencies is measured by the lock-in amplifier, as shown in Fig. 3(b). The optical intensity of each generated harmonics is less than 1% of the fundamental signal, and the total harmonic distortion THD_F (defined by the root-squared sum of all the harmonic distortion amplitude divided by the amplitude of the fundamental signal, i.e., $THD_F = \sqrt{\sum_{k\geq 2} V_k}/V_1$, where V_k is the amplitude at kth harmonic frequency) is measured to be 2.67%. The distortion originates from the nonlinear dependence of microwave frequency and the fluorescence intensity, which is a Lorentzian dip, and thus the distortion depends on the amplitude of the input signal. Importantly, this THD_F level is acceptable for the transmission of audio signals, as it can hardly be detected by a human ear [30].

Finally, we experimentally investigate our NV radio receiver operating in environmental temperature from 25 °C (i.e., 298 K) to 400 °C (673 K), where the diamond sample and the microwave microstrip shown in Fig. 1(a) are under controlled temperatures. It has been reported previously that the NV centers can operate in a wide temperature range from 6 K (Ref. [31]) to 600 K (Ref. [17]). Here, as illustrated by Eq. (1), the temperature affects the zero-field crystal field splitting of the NV centers. To demodulate a radio receiver with stable resonant microwave frequency under different temperatures, the magnetic field B_0 is used to adjust to compensate the temperature effects in a

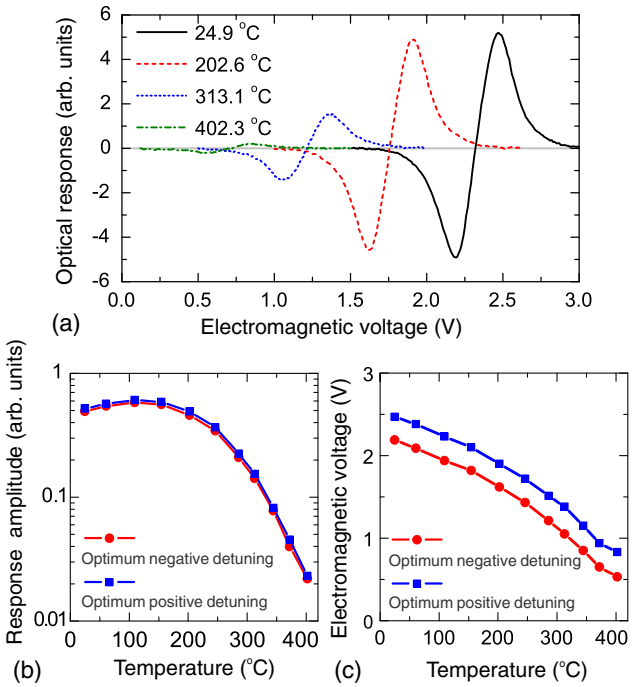

FIG. 4. (a) Optical response on the dc magnetic field B_0 under different environmental temperatures. The magnetic field B_0 is controlled by the voltage applied on the electromagnet. The sign of the optical response indicates the polarity between the NV fluorescence signal and the modulating signal. (b) The maximum responses on the environmental temperature, the response amplitudes of optimum negative and positive detuning correspond to the minimum and maximum points in (a). (c) The optimum electromagnetic voltages required to compensate the temperature shifts.

feedback loop. The NV crystal field splitting depends on the temperature T as $dD(T)/dT = -74$ kHz/K, though the exact value of the constant slightly varies between different samples with different NV densities [32]. In our case, the dc magnetic field needs to be lowered to cancel out the shift caused by the higher temperature (in the case of using the $m_s = -1$ ground-state sublevel). In the experiment, tuning of the dc magnetic field B_0 is achieved by changing the voltage applied to the electromagnet. In this experiment, the carrier frequency of the microwave signal is fixed at 2.80 GHz, the modulating signal is a 1-kHz sine wave, and the maximum frequency deviation is set to 2 MHz. As shown in Fig. 4(a), we measure the output signal under different applied electromagnet voltages and temperatures. The sign of the output signal indicates the phase relative to the modulating signal. As expected, the optimum external magnetic field B_0 changes as the temperature changes, as shown in Fig. 4(c). In addition, the signal maximum reduces as the temperature increases, as shown in Fig. 4(b). We conclude that the NV radio receiver operates up to at least 350 °C (628 K), though the amplitude of the received signal suffers at high temperatures: at 350 °C the amplitude of the signal is only one tenth of that at room temperature. This can be explained by the dynamics of NV centers: at high temperatures, the thermally activated nonradiative processes diminish the spin selectivity of the excited state intersystem crossing and the spin-dependent fluorescence vanishes out [17].

IV. CONCLUSION

In conclusion, we demonstrate a radio receiver based on NV centers in diamonds capable of demodulating the FM microwave signal and mapping it onto the amplitude-modulated fluorescent signal. The radio is tuned via a dc magnetic field, provided by an electromagnet, which selects the carrier frequency. Enjoying the robustness of diamond NV centers, we demonstrate the operation at temperatures as high as 350 °C. The required microwave power and the bandwidth of the NV centers as a transducer could be improved by designing resonant microwave circuits for specific applications or frequencies, and the excitation and collection of NV fluorescence could be enhanced by photonic structures as well. Looking ahead, we note that other atomic defects in solids can be used to realize radio receivers (or wavelength converters) in the frequency bands of interest to modern communications and quantum information processing. For example, silicon-vacancy centers in diamond have a potential for microwave-to-optical converters in the terahertz band [33], and the resonant microwave frequency can be tuned by strain.

ACKNOWLEDGMENTS

The authors thank Srujan Meesala, Young-Ik Sohn, Cheng Wang, Mengzhen Zhang, and Qiushi Guo for fruitful discussions, and Yin Feng for help in supplementary video preparation. This work was supported in part by the STC Center for Integrated Quantum Materials under NSF Grant No. DMR-1231319 and DARPA QuASAR (Grant No. HR0011-11-C-0073).

[1] H. Hertz, *Electric Waves: Being Researches on the Propagation of Electric Action with Finite Velocity through Space* (Dover Publications, New York, 1893).
[2] A. Goldsmith, *Wireless Communications* (Cambridge University Press, New York, 2005).
[3] T. Rappaport, *Wireless Communications: Principles and Practice* (Prentice Hall PTR, Upper Saddle River, 2002).
[4] C. Rutherglen and P. Burke, Carbon nanotube radio, Nano Lett. **7**, 3296 (2007).
[5] K. Jensen, J. Weldon, H. Garcia, and A. Zettl, Nanotube radio, Nano Lett. **7**, 3508 (2007).
[6] J. Bochmann, A. Vainsencher, D. D. Awschalom, and A. N. Cleland, Nanomechanical coupling between microwave and optical photons, Nat. Phys. **9**, 712 (2013).
[7] X. Zhou, F. Hocke, A. Schliesser, A. Marx, H. Huebl, R. Gross, and T. J. Kippenberg, Slowing, advancing and

switching of microwave signals using circuit nanoelectromechanics, Nat. Phys. **9**, 179 (2013).

[8] T. Bagci, A. Simonsen, S. Schmid, L. G. Villanueva, E. Zeuthen, J. Appel, J. M. Taylor, A. Sorensen, K. Usami, A. Schliesser, and E. S. Polzik, Optical detection of radio waves through a nanomechanical transducer, Nature (London) **507**, 81 (2014).

[9] T. van der Sar, F. Casola, R. Walsworth, and A. Yacoby, Nanometre-scale probing of spin waves using single-electron spins, Nat. Commun. **6**, 7886 (2015).

[10] P. Wang, Z. Yuan, P. Huang, X. Rong, M. Wang, X. Xu, C. Duan, C. Ju, F. Shi, and J. Du, High-resolution vector microwave magnetometry based on solid-state spins in diamond, Nat. Commun. **6**, 6631 (2015).

[11] V. Stepanov, F. H. Cho, C. Abeywardana, and S. Takahashi, High-frequency and high-field optically detected magnetic resonance of nitrogen-vacancy centers in diamond, Appl. Phys. Lett. **106**, 063111 (2015).

[12] N. Aslam, M. Pfender, R. Stohr, P. Neumann, M. Scheffler, H. Sumiya, H. Abe, S. Onoda, T. Ohshima, J. Isoya, and J. Wrachtrup, Single spin optically detected magnetic resonance with 60–90 GHz (*E*-band) microwave resonators, Rev. Sci. Instrum. **86**, 064704 (2015).

[13] P. Appel, M. Ganzhorn, E. Neu, and P. Maletinsky, Nanoscale microwave imaging with a single electron spin in diamond, New J. Phys. **17**, 112001 (2015).

[14] M. Chipaux, L. Toraille, C. Larat, L. Morvan, S. Pezzagna, J. Meijer, and T. Debuisschert, Wide bandwidth instantaneous radio frequency spectrum analyzer based on nitrogen vacancy centers in diamond, Appl. Phys. Lett. **107**, 233502 (2015).

[15] L. Shao, R. Liu, M. Zhang, A. V. Shneidman, X. Audier, M. Markham, H. Dhillon, D. J. Twitchen, Y.-F. Xiao, and M. Lončar, Wide-field optical microscopy of microwave fields using nitrogen-vacancy centers in diamonds, Adv. Opt. Mater. **4**, 1075 (2016).

[16] M. W. Doherty, V. V. Struzhkin, D. A. Simpson, L. P. McGuinness, Y. Meng, A. Stacey, T. J. Karle, R. J. Hemley, N. B. Manson, L. C. L. Hollenberg, and S. Prawer, Electronic Properties and Metrology Applications of the Diamond NV^- Center under Pressure, Phys. Rev. Lett. **112**, 047601 (2014).

[17] D. M. Toyli, D. J. Christle, A. Alkauskas, B. B. Buckley, C. G. Van de Walle, and D. D. Awschalom, Measurement and Control of Single Nitrogen-Vacancy Center Spins above 600 K, Phys. Rev. X **2**, 031001 (2012).

[18] R. Schirhagl, K. Chang, M. Loretz, and C. L. Degen, Nitrogen-vacancy centers in diamond: nanoscale sensors for physics and biology, Annu. Rev. Phys. Chem. **65**, 83 (2014).

[19] V. V. Dobrovitski, G. D. Fuchs, A. L. Falk, C. Santori, and D. D. Awschalom, Quantum Control over Single Spins in Diamond, Annu. Rev. Condens. Matter Phys. **4**, 23 (2013).

[20] M. Goldman, A. Sipahigil, M. Doherty, N. Yao, S. Bennett, M. Markham, D. Twitchen, N. Manson, A. Kubanek, and M. Lukin, Phonon-Induced Population Dynamics and Intersystem Crossing in Nitrogen-Vacancy Centers, Phys. Rev. Lett. **114**, 145502 (2015).

[21] G. Davies, Current problems in diamond: towards a quantitative understanding, Physica (Amsterdam) **273–274B**, 15 (1999).

[22] See Supplemental Material at http://link.aps.org/supplemental/10.1103/PhysRevApplied.6.064008 for a demonstration video of audio transmission.

[23] See Supplemental Material at http://link.aps.org/supplemental/10.1103/PhysRevApplied.6.064008 for the extensive discussion on frequency response and bandwidth of NV centers.

[24] N. B. Manson, J. P. Harrison, and M. J. Sellars, Nitrogen-vacancy center in diamond: Model of the electronic structure and associated dynamics, Phys. Rev. B **74**, 104303 (2006).

[25] S. A. Wolf, I. Rosenberg, R. Rapaport, and N. Bar-Gill, Purcell-enhanced optical spin readout of nitrogen-vacancy centers in diamond, Phys. Rev. B **92**, 235410 (2015).

[26] H. Clevenson, E. H. Chen, F. Dolde, C. Teale, D. Englund, and D. Braje, Diamond-nitrogen-vacancy electronic and nuclear spin-state anticrossings under weak transverse magnetic fields, Phys. Rev. A **94**, 021401 (2016).

[27] Y. Dumeige, M. Chipaux, V. Jacques, F. Treussart, J. F. Roch, T. Debuisschert, V. M. Acosta, A. Jarmola, K. Jensen, P. Kehayias, and D. Budker, Magnetometry with nitrogen-vacancy ensembles in diamond based on infrared absorption in a doubly resonant optical cavity, Phys. Rev. B **87**, 155202 (2013).

[28] J. P. Tetienne, L. Rondin, P. Spinicelli, M. Chipaux, T. Debuisschert, J. F. Roch, and V. Jacques, Magnetic-field-dependent photodynamics of single NV defects in diamond: An application to qualitative all-optical magnetic imaging, New J. Phys. **14**, 103033 (2012).

[29] S. Meesala, Y.-I. Sohn, H. A. Atikian, S. Kim, M. J. Burek, J. T. Choy, and M. Lončar, Enhanced Strain Coupling of Nitrogen-Vacancy Spins to Nanoscale Diamond Cantilevers, Phys. Rev. Applied **5**, 034010 (2016).

[30] K. Russell and P. A. Fryer, Loudspeakers: An Approach to Objective Listening, in *Proceedings of the 63rd Audio Engineering Society Convention* (Audio Engineering Society, Los Angeles, 1979), p. 1495.

[31] A. Batalov, V. Jacques, F. Kaiser, P. Siyushev, P. Neumann, L. J. Rogers, R. L. McMurtrie, N. B. Manson, F. Jelezko, and J. Wrachtrup, Low Temperature Studies of the Excited-State Structure of Negatively Charged Nitrogen-Vacancy Color Centers in Diamond, Phys. Rev. Lett. **102**, 195506 (2009).

[32] V. M. Acosta, E. Bauch, M. P. Ledbetter, A. Waxman, L. S. Bouchard, and D. Budker, Temperature Dependence of the Nitrogen-Vacancy Magnetic Resonance in Diamond, Phys. Rev. Lett. **104**, 070801 (2010).

[33] C. Hepp, T. Müller, V. Waselowski, J. N. Becker, B. Pingault, H. Sternschulte, D. Steinmüller-Nethl, A. Gali, J. R. Maze, M. Atatüre, and C. Becher, Electronic Structure of the Silicon Vacancy Color Center in Diamond, Phys. Rev. Lett. **112**, 036405 (2014).